Ann. Geophys., 25, 2217–2228, 2007
www.ann-geophys.net/25/2217/2007/
© European Geosciences Union 2007

Annales Geophysicae

Low frequency wave sources in the outer magnetosphere, magnetosheath, and near Earth solar wind

O. D. Constantinescu[1,2], **K.-H. Glassmeier**[1], **P. M. E. Décréau**[3], **M. Fränz**[4], **and K.-H. Fornaçon**[1]

[1]Institute for Geophysics and Extraterrestrial Physics, Braunschweig, Germany
[2]Institute for Space Sciences, Bucharest, Romania
[3]Laboratoire de Physique et Chimie de l'Environnement, Orléans, France
[4]Max-Planck-Institut für Sonnensystemforschung, Lindau, Germany

Received: 7 November 2006 – Revised: 12 August 2007 – Accepted: 18 October 2007 – Published: 6 November 2007

Abstract. The interaction of the solar wind with the Earth magnetosphere generates a broad variety of plasma waves through different mechanisms. The four Cluster spacecraft allow one to determine the regions where these waves are generated and their propagation directions. One of the tools which takes full advantage of the multi-point capabilities of the Cluster mission is the wave telescope technique which provides the wave vector using a plane wave representation. In order to determine the distance to the wave sources, the source locator – a generalization of the wave telescope to spherical waves – has been recently developed. We are applying the source locator to magnetic field data from a typical traversal of Cluster from the cusp region and the outer magnetosphere into the magnetosheath and the near Earth solar wind. We find a high concentration of low frequency wave sources in the electron foreshock and in the cusp region. To a lower extent, low frequency wave sources are also found in other magnetospheric regions.

Keywords. Magnetospheric physics (Magnetopause, cusp, and boundary layers; Magnetosheath; Plasma waves and instabilities)

1 Introduction

Numerous studies have been dedicated to the origin and nature of plasma waves in the magnetosheath and its adjacent regions. Song et al. (1990, 1992a,b) showed evidence of a standing slow mode wave in front of the magnetopause over which higher frequency mirror modes convected with the magnetosheath flow are superposed. Schwartz et al. (1996) gave a comprehensive overview of low frequency waves in the magnetosheath, pointing out the difficulties and complications faced by wave mode identification. Their conclusion is that Alfvén/ion-cyclotron (AIC) and mirror modes are dominant throughout the magnetosheath. Most of the times the waves in the magnetosheath are not pure modes but rather a mixture of wave modes. Hubert et al. (1998) suggests that the distance from the bowshock is a key parameter determining the plasma waves nature. During a crossing of the Earth's magnetosheath they found compressive and AIC modes from the ramp to the undershoot of an oblique shock, pure AIC waves in the outer magnetosheath, a mixture of AIC and mirror modes in the middle magnetosheath and pure mirror modes in the inner magnetosheath. Narita and Glassmeier (2005) used magnetic field data from Cluster spacecraft (Escoubet et al., 1997) to determine the wave vectors across the magnetosheath. The multi point measurements allowed for Doppler correction and for the determination of the dispersion relation, facilitating the wave mode identification. They found a mixture of ion-cyclotron and mirror modes close to the shock, then a region where mirror modes were dominating and finally, close to the magnetopause they found distorted mirror modes. Comparing the observed transport ratios and polarization properties with the values given by a linear kinetic model, Blanco-Cano and Schwartz (1997) found left hand polarized Alfvén and right hand polarized magnetosonic waves in the proton foreshock. However, they stress the differences between the observed waves and theoretical predictions.

It is the aim of this work to systematically study the spatial distribution of wave sources along a magnetosheath crossing by Cluster. One of the most suitable tools for this task is the source locator (Constantinescu et al., 2006) which is the generalization of the wave telescope/k-filtering technique (Pinçon and Lefeuvre, 1991; Lefeuvre and Pinçon, 1992; Motschmann et al., 1995; Glassmeier et al., 2001; Sahraoui et al., 2003) to spherical waves.

Correspondence to: O. D. Constantinescu
(d.constantinescu@tu-bs.de)

Published by Copernicus Publications on behalf of the European Geosciences Union.

2 Source locator: theory

The source locator uses simultaneous measurements at different points in space to decompose a wave field into spherical wave components. The difference from the wave telescope lies in the choice of spherical waves rather than plane waves as basis functions.

Let $\boldsymbol{X}^s(t)=\left(x_1^s(t),\ldots,x_L^s(t)\right)^{\mathsf{T}}$, be a set of measurements performed at the position $\boldsymbol{r}^s$. The superscript $s=1,\ldots,S$ refers to the sensor in the array. The superscript T denotes the transposition operation, therefore $\boldsymbol{X}^s(t)$ is an $L\times 1$ column vector. It can represent one or more physical quantities such as the magnetic field magnitude ($X^s(t)=B(\boldsymbol{r}^s,t)$) in which case $L=1$, the magnetic field vector ($\boldsymbol{X}^s(t)=\boldsymbol{B}(\boldsymbol{r}^s,t)$) in which case $L=3$, a combination of electric and magnetic field ($\boldsymbol{X}^s(t)=\left(c\boldsymbol{B}^{\mathsf{T}}(\boldsymbol{r}^s,t),\boldsymbol{E}^{\mathsf{T}}(\boldsymbol{r}^s,t)\right)^{\mathsf{T}}$), in which case $L=6$, or other coherent quantities. Since the time resolution is usually good enough, we can move from the time to the frequency domain:

$$\tilde{\boldsymbol{X}}^s(\omega)=\frac{1}{2\pi}\int \boldsymbol{X}^s(t)e^{i\omega t}\mathrm{d}t \tag{1}$$

We assume the measured wave field is a superposition of N orthogonal elementary waves w:

$$\tilde{\boldsymbol{X}}^s(\omega)=\sum_{n=1}^{N}\boldsymbol{C}(\omega,\boldsymbol{q}_n)w^s(\boldsymbol{q}_n) \tag{2}$$

Each elementary wave is characterized by the set of parameters $\boldsymbol{q}=(q_1,\ldots,q_M)^{\mathsf{T}}$ depending on our choice of the set $\{w\}$. Our goal is to find the coefficients $\boldsymbol{C}(\omega,\boldsymbol{q}_n)$ associated with each elementary wave.

We group the measurements from all S sensors into the $(LS\times 1)$ vector:

$$\tilde{\boldsymbol{X}}(\omega)=\left(\tilde{\boldsymbol{X}}^{1\,\mathsf{T}}(\omega),\ldots,\tilde{\boldsymbol{X}}^{S\,\mathsf{T}}(\omega)\right)^{\mathsf{T}} \tag{3}$$

and the elementary waves into the $(LS\times L)$ matrix:

$$\mathbf{W}(\boldsymbol{q}_n)=\left(\mathbf{I}w^1(\boldsymbol{q}_n),\ldots,\mathbf{I}w^S(\boldsymbol{q}_n)\right)^{\mathsf{T}} \tag{4}$$

where $\mathbf{I}$ is the $L\times L$ unit matrix. With these notations, Eq. (2) becomes:

$$\tilde{\boldsymbol{X}}(\omega)=\sum_{n=1}^{N}\mathbf{W}^{\mathsf{T}}(\boldsymbol{q}_n)\boldsymbol{C}(\omega,\boldsymbol{q}_n) \tag{5}$$

and the orthogonality relation $\boldsymbol{w}^{\dagger}(\boldsymbol{q})\boldsymbol{w}(\boldsymbol{q}')=\delta(\boldsymbol{q}-\boldsymbol{q}')$ becomes:

$$\mathbf{W}(\boldsymbol{q})\mathbf{W}^{\dagger}(\boldsymbol{q}')=\mathbf{I}\delta(\boldsymbol{q}-\boldsymbol{q}') \tag{6}$$

We define the array output as:

$$\boldsymbol{X}_{\mathrm{A}}(\omega,\boldsymbol{q})=\mathbf{W}^{\dagger}(\boldsymbol{q})\tilde{\boldsymbol{X}}(\omega) \tag{7}$$

The $\dagger$ symbol above stands for the Hermitian adjoint: $\boldsymbol{x}^{\dagger}=\boldsymbol{x}^{\star\,\mathsf{T}}$. Substituting the decomposition (5) and the orthogonality relation (6) into Eq. (7) we find:

$$\boldsymbol{X}_{\mathrm{A}}(\omega,\boldsymbol{q})=\sum_{n=1}^{N}\boldsymbol{C}(\omega,\boldsymbol{q}_n)\delta(\boldsymbol{q}_n-\boldsymbol{q}) \tag{8}$$

The array power $\mathbf{P}$ is defined as the squared norm of the array output:

$$\mathbf{P}(\omega,\boldsymbol{q})=||\boldsymbol{X}_{\mathrm{A}}(\omega,\boldsymbol{q})||^2=\mathbf{W}^{\dagger}(\boldsymbol{q})\mathbf{M}(\omega)\mathbf{W}(\boldsymbol{q}) \tag{9}$$

where the measurements matrix $\mathbf{M}$ is defined as:

$$\mathbf{M}(\omega)=\tilde{\boldsymbol{X}}(\omega)\tilde{\boldsymbol{X}}^{\dagger}(\omega) \tag{10}$$

The contribution of the elementary wave w associated with the set of parameters $\boldsymbol{q}$ to the total wave field is given by the trace of the array power $\mathbf{P}(\omega,\boldsymbol{q})$.

When the number S of sensors is sufficient, we can use the above defined power to perform the decomposition of the measured wave field. This method is known as the beamformer technique (Pillai, 1989). However, the Cluster constellation consists of only four spacecraft. This renders the system $\{w\}$ far from complete, leading to artificial contributions to the power at points in the parameter space which do not correspond to any real wave source. A remedy is to minimize these contributions while keeping the power corresponding to the real wave sources unmodified. This is accomplished by Capon's minimum variance estimator (Capon et al., 1967) which results in a re-definition of the array power as:

$$\mathbf{P}(\omega,\boldsymbol{q})=\left[\mathbf{W}^{\dagger}(\boldsymbol{q})\mathbf{M}^{-1}(\omega)\mathbf{W}(\boldsymbol{q})\right]^{-1} \tag{11}$$

Now we only have to compute the power over a domain in the parameter space $\{q_n\}$ and analyze its trace. If we identify strong maxima, their coordinates indicate the parameter sets $\boldsymbol{q}$ corresponding to the dominant waves.

Up to this point we have not specified a particular set $\{w(\boldsymbol{q})\}$. If we chose the plane waves representation

$$w_s(\boldsymbol{k})=\frac{1}{\sqrt{S}}e^{i\boldsymbol{k}\cdot\boldsymbol{r}_s} \tag{12}$$

we obtain the wave telescope/k-filtering technique which determines the wave vector $\boldsymbol{k}$ (Pinçon and Lefeuvre, 1991; Motschmann et al., 1995).

Figure 1 shows a comparison between the beamformer and the wave telescope techniques. Both methods are applied to artificial data representing a plane wave measured with four sensors arranged in a regular tetrahedron configuration. The resulting array power is plotted as a function of the longitude angle of the $\boldsymbol{k}$ vector. For both methods the power maximizes at the right longitude (40°). However, the power computed with the wave telescope method has a much sharper maximum than the power computed with the beamformer technique.

For the source locator we choose the spherical waves representation

$$w_s(k, \boldsymbol{r}) = C \frac{1}{|\boldsymbol{r} - \boldsymbol{r}_s|} e^{ik|\boldsymbol{r}-\boldsymbol{r}_s|} \tag{13}$$

where $\boldsymbol{r}$ is the wave source position and C is a normalization coefficient:

$$C = \left(\sum_{s=1}^{S} \frac{1}{|\boldsymbol{r} - \boldsymbol{r}_s|^2} \right)^{-1/2} \tag{14}$$

The trace of the array power $\mathbf{P}(k, \boldsymbol{r})$ represents in this case the contribution to the measured wave field of the wave source situated at the position $\boldsymbol{r}$ and emitting a wave with the wave number k (Constantinescu et al., 2006).

3 Magnetosheath crossing

The time interval selected for this study is during an outbound magnetosheath crossing on 18 February 2002. Parts of this interval already have been analyzed in several papers giving us an opportunity for comparison. Using the k-filtering technique Sahraoui et al. (2003) investigate a magnetic field data interval of 164 s in lengths, in the inner magnetosheath, starting from from 05:34 UT. The power spectrum for frequencies between 350 and 12 500 mHz suggests a turbulence cascade and more wave modes are found for each given frequency. They find that a mirror mode propagating at an angle around 60° to the background magnetic field dominates the wave field but there are also contributions from Alfvén, slow, and cyclotron wave modes. For the same data interval but for lower frequencies, Sahraoui et al. (2004) find similar results, with the mirror modes propagating closer to the orthogonal direction at 80°. Tjulin et al. (2005) confirm the presence of mirror modes for the same interval by analyzing the electric field fluctuations after using both magnetic and electric field as input for the k-filtering. Walker et al. (2004) compare the results obtained via k-filtering with those obtained via phase differencing method (Balikhin et al., 1997) applied to the same 164 s data interval. They find a mixture of slow, Alfvén and mirror waves with their wave vectors close to the orthogonal direction to the average magnetic field. They stress the "highly changeable" nature of the waves detected during this interval. At low frequencies, the mirror mode is found to be dominating. Narita and Glassmeier (2005) analyze four different intervals for this crossing: one in the inner magnetosheath, one in the middle magnetosheath, one in the outer magnetosheath and one in the ion foreshock region. They use the wave telescope technique to determine the wave vectors which are then used to find the experimental dispersion relation. In the foreshock they find waves propagating slightly oblique (20°−30°) to the background magnetic field and a minority population of orthogonal propagating waves. From the interpretation of the dispersion relation they suggest the detected waves in the foreshock are ion-whistler and beam-resonant mode. The waves in the outer magnetosheath have various propagation angles from oblique to orthogonal and it is suggested that they are mirror modes with small contribution from other modes, perhaps ion-cyclotron. In the middle magnetosheath they find orthogonal propagating, linear polarized waves, interpreted as mirror modes which are convected with the plasma flow into the inner magnetosheath region where they coexist with the slow mode.

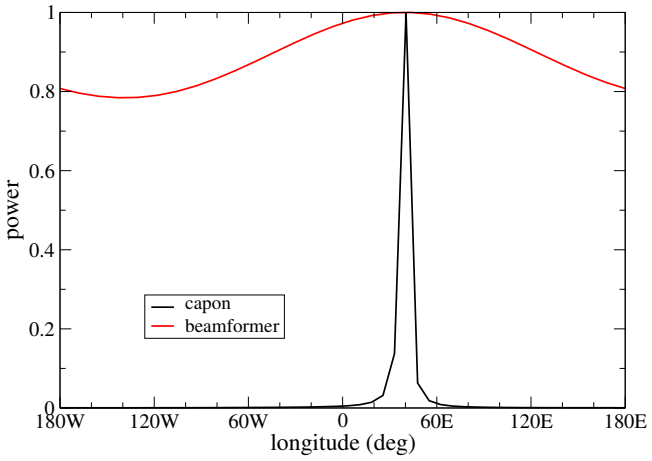

Fig. 1. Comparison between the beamformer (red) and the Capon (black) techniques for one plane wave detected with a regular tetrahedron array.

3.1 Data and geophysical conditions

During the magnetosheath crossing, the interplanetary magnetic field pointed northward and the average shock angle was around 17° (Narita and Glassmeier, 2005). The tetrahedron configuration changes during this time interval but remains reasonably close to a regular tetrahedron with a characteristic separation distance of about 100 km.

An overview of the plasma and field parameters during this time can be seen in Fig. 2 generated by the Cluster Science Data Center. The components of the magnetic field measured by the Flux Gate Magnetometer (FGM) (Balogh et al., 1997) are represented in more detail in Fig. 3.

The different regions crossed by the Cluster constellation are marked by the colored rectangles. From 02:10 to 03:30 UT the Cluster fleet is in the cusp region. Between 03:30 and 05:00 UT it samples the outer magnetosphere between the cusp and the magnetosheath. It enters the magnetosheath at 05:00 UT and leaves it at 07:45 UT. The first traversal of the ion foreshock occurs between 07:45 and 09:00 UT followed by a short visit into the electron foreshock between 09:00 and 10:15 UT. Finally, at 10:15 UT, the spacecraft formation returns into the ion foreshock and remains there until the end of the data interval at 12:00 UT.

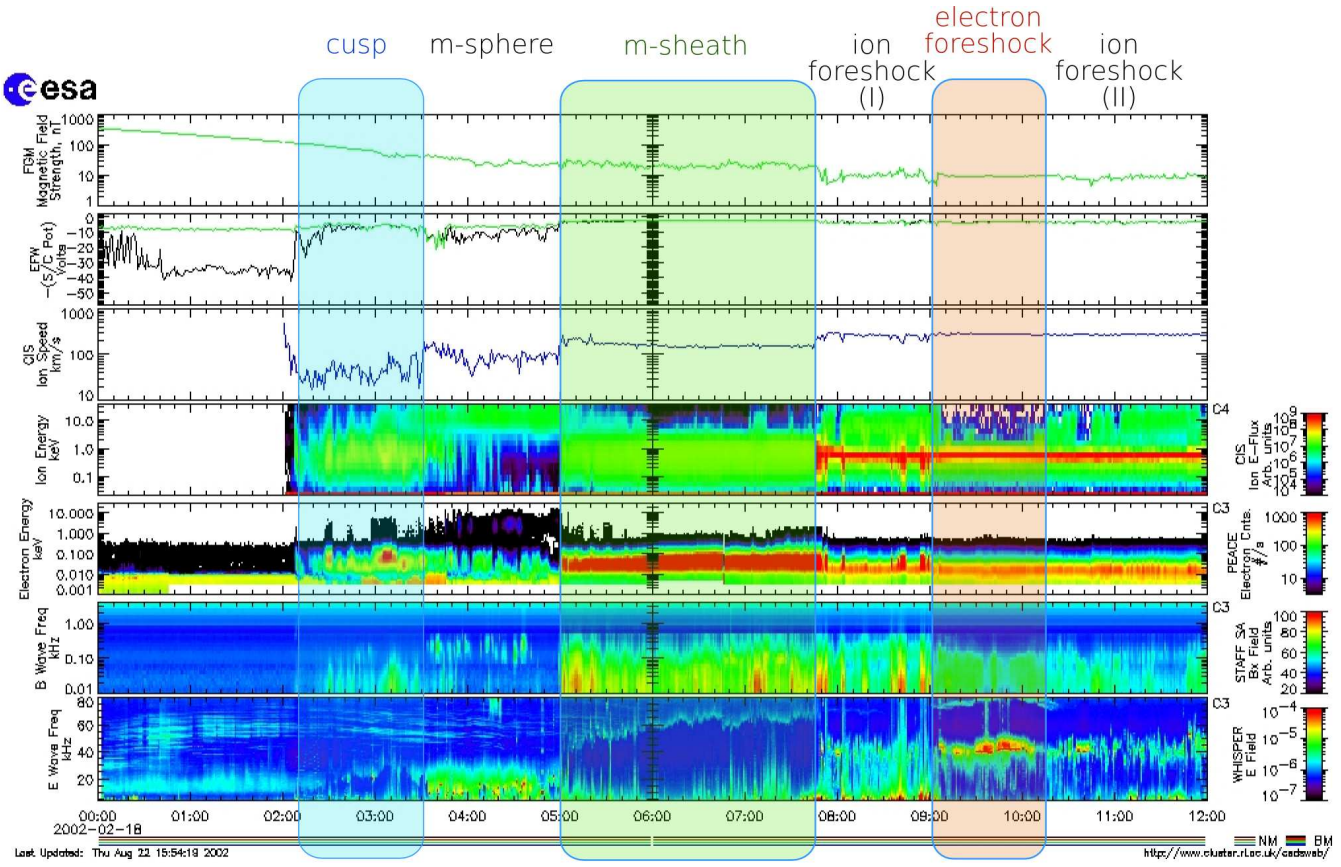

Fig. 2. Overview of field and plasma parameters measured by Cluster 3 on 18 February 2002. From top to bottom: The magnetic field magnitude (FGM), the spacecraft potential (ASPOC), the ion speed (CIS/HIA), the ions energy (CIS/HIA), the electrons energy (PEACE), the magnetic field waves power (STAFF), and the electric field waves power (WHISPER). Courtesy ESA, from Cluster Active Archive (http://caa.estec.esa.int/caa/).

The enhancement of the low energy ($\approx$0.1 keV) electrons density seen in the PEACE (Johnstone et al., 1997) data, the decrease in the energy of the main ion population measured by CIS (Rème et al., 2001), as well as the small decrease in the magnetic field amplitude visible in the FGM data around 03:10 indicate the cusp traversal. The high level of continuum noise below 30 kHz in the WHISPER (Décréau et al., 1997) spectrogram from 03:30 to 05:00 UT is likely due to trapped particles in the magnetosphere between cusp and magnetosheath. The transition between the magnetosphere and the magnetosheath and between the magnetosheath and the foreshock can easily be seen both in the ion CIS data and in the electron PEACE data. In the WHISPER data we identify electrostatic Langmuir waves through almost the whole interval. Their frequency is proportional to the square root of the electron density: between 15 and 30 kHz in the cusp and magnetosphere regions, around 60 kHz in the magnetosheath and around 40 kHz in the foreshock.

The electron foreshock is indicated by the increase in the Langmuir wave activity and by the presence of waves with twice the electron plasma frequency, the so-called $2f_p$ emissions (see Tsurutani and Rodriguez, 1981; Kasaba et al., 2000).

During the ion foreshock (I) interval, the presence of weak Langmuir and $2f_p$ waves suggests that the constellation was already close to the electron foreshock. As we will see later, the larger distance to the foreshock boundary causes the two ion foreshock intervals to have different properties.

3.2 Typical samples

Before we discuss the statistics of waves detected during the selected time interval we shall have a look at typical array power plots for each of the magnetospheric regions encountered by Cluster during the selected interval.

To compute the array power (Eq. 11) we use 1-s resolution magnetic field data provided by the FGM instrument onboard Cluster spacecraft. All three components of the magnetic field are used, resulting in a 12×12 measurements matrix **M**. To optimize the fast Fourier transform performance, the data intervals are chosen to be 512 s in length. We compute the array power over a grid in the space $\{k, \rho, \theta, \varphi\}$,

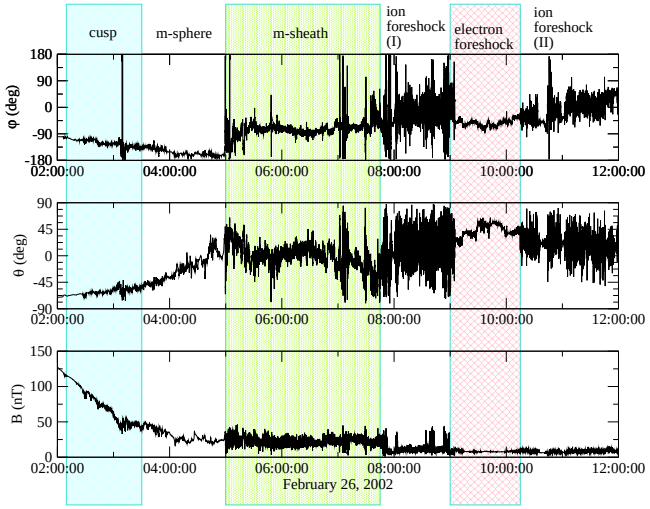

Fig. 3. The magnetic field in spherical GSE coordinates measured by Cluster 1 on 18 February 2002. Different regions are marked by colored rectangles.

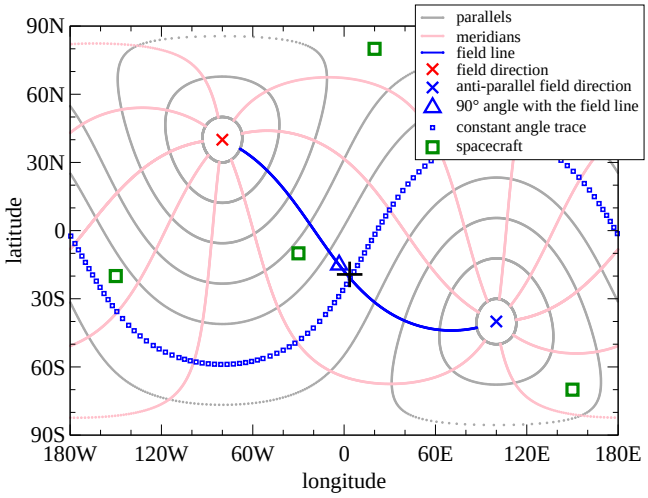

Fig. 4. Sketch of a typical longitude latitude representation of the array power. The direction to the Sun is in the center of the map. A set of parallel and meridian lines associated with the magnetic field direction is shown for reference. The magnetic field line going through the wave source follows a meridian line. The directions making the same angle with the magnetic field as the detected wave gather along a parallel line.

where $k \in (0, k_{\text{Nyquist}})$ is the wave number, $\rho \in (0, 30 d_{\min})$ is the distance from the configuration center ($d_{\min}$ is the minimum distance between two spacecraft), $\varphi \in (-\pi, \pi]$ and $\theta \in [-\pi/2, \pi/2]$ are the longitude and respectively latitude angles in the GSE system translated to the spacecraft configuration center. Each dimension is divided into 30 grid points which results in a power array with 30^4 elements. To present this four-dimensional array power we use two bi-dimensional slices which include the power maximum: one latitude-longitude plot at fixed distance and wave number, and one distance-wave number plot at fixed latitude and longitude.

The longitude-latitude plots are equirectangular projections and besides the color coded array power they contain a number of guiding elements shown for convenience in Fig. 4. The green squares mark the positions of the spacecraft. The mean magnetic field direction is marked with a red **x** sign and the corresponding anti-parallel direction is marked with a blue (in Fig. 4) or yellow (in the subsequent plots) **x** sign. The solid line between these two symbols represents the magnetic field line which goes through the identified wave source (the power maximum). On this line there is a triangle symbol which indicates the point on the magnetic field line which is closest to the spacecraft configuration center. The position of the power maximum on the magnetic field line shows the wave propagation angle. If the maximum is close to the triangle symbol then the local propagation direction of the detected wave is orthogonal to the magnetic field. If the maximum power is close to one of the **x** signs then we are detecting a parallel/anti-parallel propagating wave. The plasma flow line through the source (not shown in Fig. 4 but present in the subsequent figures) is represented by the dashed line. A triangle symbol on this line has a similar meaning with the corresponding symbol on the magnetic field line. Finally, there is a dotted line representing all directions making the same angle with the background magnetic field as the line of sight to the source. They generate a cone around the line of sight to the source.

Figure 5 shows the array power as derived by the source locator for sample intervals in the ion foreshock (II), electron foreshock, and ion foreshock (I). Figure 6 completes the picture with power plots from the magnetosheath, magnetosphere, and cusp samples.

In the ion foreshock (II) sample the source locator detects a remote source with a frequency of 83 mHz in the spacecraft frame, a wave length around 3000 km, and an angle of 148° with the background magnetic field. The frequency in the plasma rest frame is found after the Doppler shift correction to be −20 mHz. The negative frequency means that in the plasma rest frame the wave propagates in the opposite direction as detected in the spacecraft frame ($\boldsymbol{k} \rightarrow -\boldsymbol{k}$). The wave propagates against the solar wind but because of the relatively low phase speed (around 60 km/s) it is convected by the flow.

As opposed to the ion foreshock (II) sample, the electron foreshock sample reveals a close source positioned at only 244 km from the array center. This suggests that waves are locally generated in this region. The wave propagates orthogonal to the magnetic field (θ=96°) with a spacecraft frame frequency of 124 mHz. If we assume the wave source is convected with the plasma flow, the Doppler corrected frequency becomes −46 mHz. The phase speed is the same as for the ion foreshock (II) sample, 60 km/s.

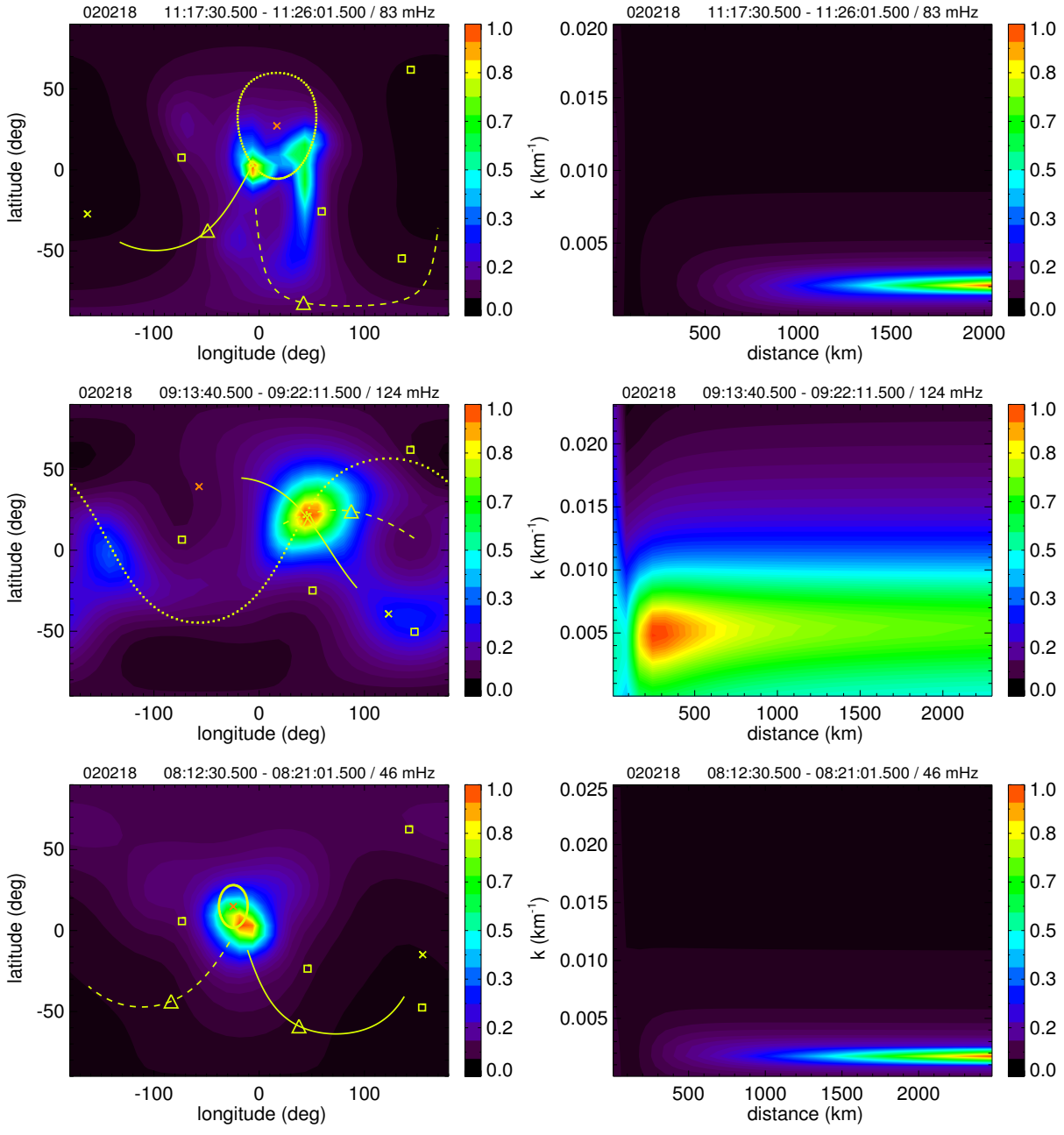

Fig. 5. Array power for data samples in different magnetospheric regions. From top to bottom: ion foreshock (II), electron foreshock, and ion foreshock (I). The ion foreshock (II) wave propagates oblique from a remote source. The local generated electron foreshock wave propagates orthogonal to the mean magnetic field. In the ion foreshock (I) a parallel propagating plane wave is detected.

With an angle of 167° to the background magnetic field, the ion foreshock (I) wave is propagating almost parallel to the ambient magnetic field. The source is remote and the latitude-longitude plot is very clean, indicating a wave with a well defined propagation direction. The Doppler correction changes the detected frequency of 48 mHz to a negative rest frame frequency of −20 mHz. Taking into account the wave length of about 3500 km, the phase speed is 70 km/s.

The wave detected in the magnetosheath sample propagates with an angle of 105° to the average magnetic field. It is also a plane wave, the distance to the source being larger than 30 times the inter-spacecraft distance. The detected frequency of 109 mHz becomes −13 mHz in the plasma rest frame. With a wave length of about 1000 km this yields a phase speed of just 12 km/s.

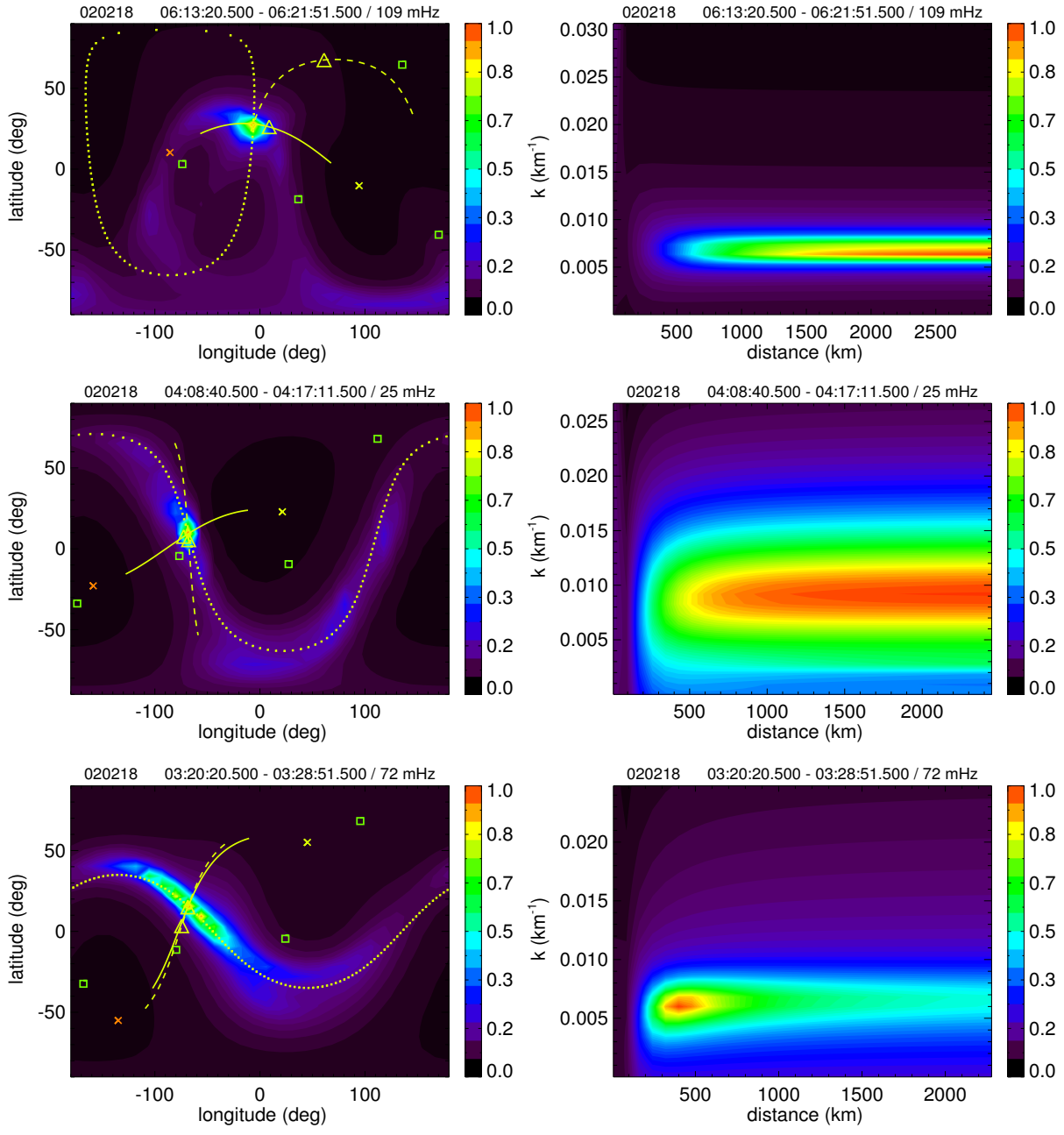

Fig. 6. Array power for data samples in different magnetospheric regions: From top to bottom: magnetosheath, magnetosphere, and cusp region. The magnetosheath wave propagates almost orthogonal to the mean magnetic field. This wave comes from a remote source. A remote source of orthogonal propagating waves is detected in the magnetosphere. Note the increased power along the "90 degrees line". The cusp wave also propagates along the orthogonal direction to the mean magnetic field. Most of the power comes from a close source. However, there is an important contribution from an orthogonal propagating waves background.

Inside the magnetosphere we detect a remote source emitting a wave with a wave length of around 700 km, a frequency of 25 mHz in the spacecraft frame, propagating at an angle of 93° with the mean magnetic field. The plasma flows almost orthogonal to the line of sight to the source, minimizing the Doppler effect. The plasma rest frame frequency of this wave is 12 mHz. The phase speed is as low as 8 km/s.

In the cusp sample, the source locator detects once more a close wave source about 400 km away from the configuration center, emitting a wave which propagates orthogonal to the background magnetic field (θ=91°). The wave length is around 1000 km and the frequency in the spacecraft frame is 72 mHz. Because the plasma flows with lower velocities in the cusp and the wave propagation direction is

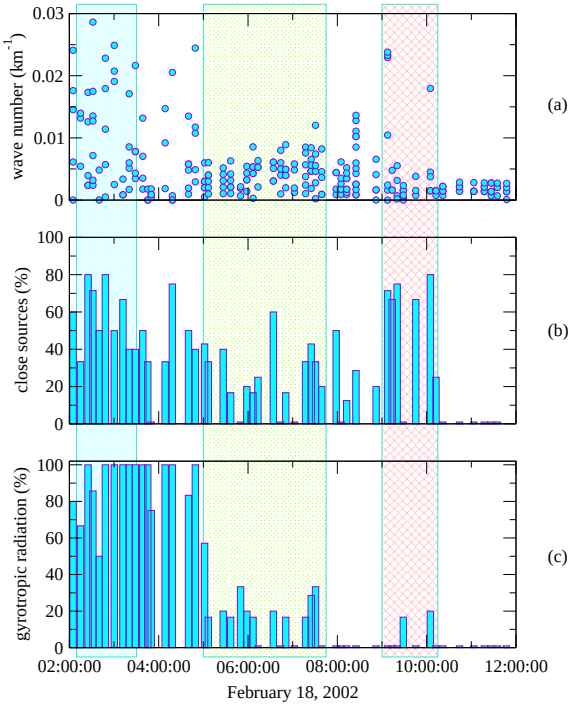

Fig. 7. The wave number **(a)**, the percent of close sources **(b)**, and the percent of samples showing gyrotropic wave fields **(c)**. The statistics are based on a total number of 264 samples distributed over 52 time intervals.

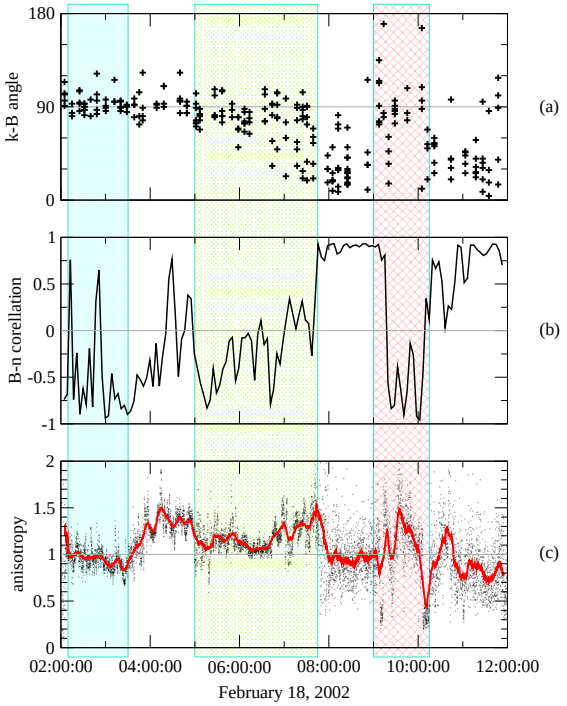

Fig. 8. The propagation angle with respect to the background magnetic field **(a)**, the correlation between the magnetic field magnitude and the plasma density **(b)**, and the proton temperature anisotropy **(c)**. The anisotropy plot shows both the 4-s resolution anisotropy (scattered black dots) and the 10-min running average (red line).

almost orthogonal to the plasma flow, the Doppler corrected frequency remains positive, taking a value of 45 mHz. The corresponding phase speed is 47 km/s.

A striking feature of the latitude-longitude plot for both the cusp and the magnetosphere sample is the almost perfect alignment of the array power maximum with the line marking all directions orthogonal to the background magnetic field. This means the source locator detects waves propagating in all directions in a plane orthogonal to the mean magnetic field. The wave field consists of a dominating wave coming from the identified close source superposed on a more or less isotropic background field of orthogonal propagating waves. Such wave field suggests that the Cluster constellation is immersed in an active region of homogeneously distributed sources generating orthogonal propagating waves. In our statistical analysis we have encountered many similar situations especially in the cusp and the outer magnetosphere regions. We call the wave field gyrotropic when the array power maximizes for all directions making a certain angle with the background magnetic field.

3.3 Statistical study

We now apply the source locator to 52 data intervals, each 512 s in length, with a time resolution of 1 s, distributed over the time period 02:00–12:00 UT on 18 February 2002. Each interval is Fourier analyzed and the source locator is applied for several frequencies for which the wave power has significant maxima. In total there are 264 samples for various time intervals and frequencies, giving an average of five frequency samples for each data interval.

In the Fig. 7a we show the wave lengths as determined by the source locator. The colored boxes mark the different magnetospheric regions in the same way as in Fig. 3. For each data interval, the percent of the sources detected close to the spacecraft array (distance less than 1500 km) is shown in Fig. 7b. The percent of samples exhibiting gyrotropic wave fields is shown in Fig. 7c. Averages over each region are given in Table 1.

Figure 8 displays the wave propagation angle with respect to the background magnetic field for the 264 considered samples, the correlation between the magnetic field and the plasma density, and the temperature anisotropy ($A{=}T_{\perp}/T_{||}$) as resulted from the Cluster 1 CIS/CODIF measurements of the proton temperatures.

We detect distinct (as opposed to gyrotropic wave field) long wave length plane waves in the ion foreshock (II). Most waves propagate oblique, at an angle around 30° to the average magnetic field. A minority of orthogonal propagating waves is also present. The magnetic field variations are in phase with the plasma density and the anisotropy is variable

showing values both above and below one. These waves might be fast mode waves.

The character of the waves changes dramatically in the electron foreshock. Now a few waves with short wave lengths are mixed with the long wave lengths waves and more than half of the waves come from close sources. A slight indication of gyrotropy suggests an increased spatial density of the wave sources. The waves have scattered propagation directions with a majority of orthogonal propagating waves. The magnetic field becomes anti-correlated with the plasma density and the temperature anisotropy rises up to a value of 1.5 from a low of 0.5. The waves here might be slow or mirror modes mixed with a minority of AIC waves.

In the ion foreshock (I) we encounter different wave characteristics again. Even though there are fewer close sources than in the electron foreshock, their contribution is still significant. Waves are generated near to as well as remote from the spacecraft configuration. The propagation is once again oblique with an average angle of 20° to the mean magnetic field. The magnetic field is now highly correlated with the particle density and the plasma temperature is almost isotropic. The AIC and fast mode are compatible with these wave properties.

About one quarter of the magnetosheath waves are generated within a distance of 2000 km from the spacecraft configuration center. More samples show gyrotropic fields, indicating more stable waves than in the foreshock. The average wave length increases as we move from the shock towards the magnetopause. A transition is also observed in the waves propagation direction. Close to the shock we detect waves propagating at various angles to the background magnetic field. This angle distribution smoothly changes to orthogonal propagation in the vicinity of the magnetopause. The correlation between the magnetic field and the plasma density has a descending trend, from values indicating no significant correlation in the outer magnetosheath, to negative values indicating anti-correlation in the inner magnetosheath. The plasma temperature anisotropy is variable during the magnetosheath crossing. First it fluctuates around 1.3 in the outer magnetosheath, it decreases close to unity in the middle magnetosheath, and fluctuates around a value of 1.1 in the inner magnetosheath. These properties are consistent with mirror mode growing while being convected by the plasma flow. The waves close to the shock might be a mixture of AIC and mirror modes, gradually changing to a mixture of mirror and slow modes close to the magnetopause.

The waves in the outer magnetosphere have a broader distribution of the wave lengths and propagate orthogonal to the mean magnetic field. Almost half of them originate from close sources and over 90% of the wave fields measured here are gyrotropic. No clear correlation between the plasma density and the magnetic field is observed close to the magnetopause. Toward the cusp the magnetic field tends to be anti-correlated with the plasma density. The temperature anisotropy indicates possible mirror mode activity.

Table 1. The average number of close sources and the average number of gyrotropic samples for each magnetospheric interval.

	close sources (%)	gyrotropic waves (%)
ion foreshock (II)	0	0
electron foreshock	55	5
ion foreshock (I)	22	0
magnetosheath	25	18
magnetosphere	40	94
cusp	57	89

The cusp waves are highly gyrotropic and more than half of them come from close sources. Both features are consistent with a region where waves are locally produced by a homogeneous distribution of point sources. The wave propagation directions remain orthogonal to the mean magnetic field while the correlation between the magnetic field and the plasma density is mostly negative with occasional positive values. The plasma temperature in the cusp region is nearly isotropic with a slight decreasing tendency towards the end of the time subinterval. These facts suggest that slow mode waves are generated in and populating the cusp.

The distribution of the distances to the sources for a magnetospheric region carries information about the spatial distribution of the wave sources within that region. For instance, if we assume the sources are uniformly distributed in space, then the distribution of the distances to the sources given by the source locator will reflect the distribution of the distance between a wave source and its first order neighbor. The top panel in Fig. 9 shows the distance to each source detected by the source locator. The points gathered at large distances aligned at the top of this figure are remote sources. For these sources the array power maximized at the maximum distance in the scan domain, indicating that the distance to these sources is too large to be determined by the source locator. The bottom panel of the Fig. 9 shows a histogram of the distribution of the distances to sources. Gray colour is for the whole data interval while coloured bars are for different magnetospheric regions. If we assume uniform distribution of wave sources across each magnetospheric region, from the cusp histogram we find the source characteristic distance (defined as the most probable distance between two sources) in the cusp close to 250 km. Similarly, the source characteristic distance in the magnetosheath is 750 km. The electron foreshock histogram seems to be split between the cusp and the magnetosheath characteristic distances, suggesting two different regimes in the electron foreshock. The other magnetospheric regions' histograms are not conclusive.

The interpretation of these statistical results is not always straightforward. For instance, it would be tempting to interpret the ratio between close and remote sources in Fig. 7b as representing the wave source density per unit volume. It

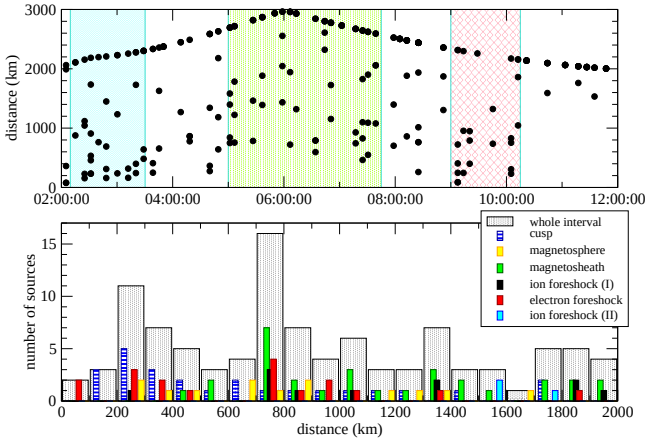

Fig. 9. Distances to the sources. Top panel: distances to the wave sources for all detected sources during the interval. Bottom panel: Histogram of the distances to the sources for the entire data interval and for specific regions.

does, but not in an absolute way. A strong damping of the waves would increase this ratio because the remote sources would simply become "lost in the fog" and the source locator would only detect close sources. The same is valid for the gyrotropy. High gyrotropy can be achieved either through high spatial density of wave sources, or through low damping of the waves. The transition of waves from one mode to another would decrease the wave field gyrotropy. However, combining the statistical information about the close-remote ratio, the gyrotropy, and the source characteristic distance gives us sufficient confidence in our interpretation.

The highly changeable nature of the waves for this particular interval was already noticed by Walker et al. (2004). The nature of the waves differs from interval to interval and from frequency to frequency for a given interval. Though we did not investigate the secondary power maxima, there is evidence (Sahraoui et al., 2003) that even for a given interval and given frequency, significant mixing of wave modes occurs. As pointed out by Sahraoui et al. (2003), this results in a mix of polarizations creating difficulties in wave mode identification.

4 Conclusions

By analyzing the curvature of the wave fronts, the source locator provides the distance to the wave sources. The spatial distribution of the wave sources allows one to differentiate between active regions where waves are locally generated and passive ones where the detected waves are just propagating through. All the magnetospheric regions covered here show a certain degree of activity. The cusp and the outer magnetosphere seem to be particularly active regions with high spatial density of wave sources. The magnetosheath is as well very active but the characteristic distance between wave sources is larger here. The characteristic distance for the foreshock is uncertain. Nevertheless, the high percentage of close sources found in the electron foreshock suggest that the electron foreshock is as well very active. Interestingly, in the ion foreshock we found only a few low frequency wave sources. This is contrary to what we expect. The counter-streaming ions should locally generate waves through the beam instability. Are there quiet regions in the ion foreshock? Is this a temporal effect indicating intermittence in the wave generation? Is this an isolated case which occurred just for this particular crossing? Or maybe the ion beam instability only determines mode conversion and further growth of the already present small amplitude waves propagating from the electron foreshock. We favor the last possibility but we cannot exclude any of the above cases.

A possible scenario of the solar wind-magnetosphere interaction for the considered interval is: The solar wind flow encounters the counter-streaming reflected electrons in the electron foreshock region as a first sign of the shock ahead. The resulting interaction excites small amplitude mirror mode and AIC waves. When the electron foreshock waves penetrate into the ion foreshock, mode conversions triggered by the ion beam instability occur. High amplitude AIC and fast magnetosonic waves populate this region. Most of them originate in and close to the electron foreshock. They continuously gain energy from the reflected ions as they travel across the ion foreshock. After the solar wind crosses the bowshock, the wave lengths become gradually larger, waves are locally generated, and the AIC population extinguishes in favor of the mirror structures. Behind the magnetopause, mirror waves fill the more homogeneous region of the magnetosphere between the magnetosheath and the cusp. Slow mode waves are generated close to each other in the cusp region.

The above scenario for the magnetosheath is in good agreement with previous studies (Song et al., 1990; Schwartz et al., 1996; Hubert et al., 1998) which describe the magnetosheath waves as a mixture of AIC and mirror modes evolving in favor of the mirror modes as they are convected with the flow toward the magnetopause.

The study of Narita and Glassmeier (2005) focused on the ion foreshock (I) – magnetosheath part of the interval presented in this work, mostly agrees with our findings. It is only the inner magnetosheath region where slightly different conclusions are reached. While our analysis suggests a steady evolution to more mirror-like waves toward the magnetopause, Narita and Glassmeier (2005) find that the waves in the middle magnetosheath are closer to mirror modes than the waves in the inner magnetosheath. They regard this as a consequence of the interaction with the magnetopause which is distorting the mirror structures. There are two possible reasons for this minor discrepancy we can think of. First, the way of sample selection differs. Narita and Glassmeier (2005) are treating the power spectrum as a turbulent-like spectrum. Consequently, they do not select the frequencies

based on their relative contribution to the wave field. On the contrary, we always select frequencies for which the power presents local peaks. Since indeed, most of the time there are not outstanding local maxima in the Fourier spectrum, but rather small local maxima (an exception being the foreshock region), this difference in sample selection should not influence much the statistical results. However, there is a fundamental difference between the plane waves representation of the wave telescope used by Narita and Glassmeier (2005) and the spherical waves representation of the source locator. When the wave field consists of a mixture of locally generated waves and waves coming from remote locations, the source locator will detect the wave with the highest energy density, most probably the wave locally generated. On the contrary, the wave telescope will detect the remote generated wave rather the wave generated locally even if the energy density of the locally generated wave is much higher than the energy density of the remote generated wave. This is due to the fact that the large curvature of the locally generated wave prevents the wave telescope to recognize it as a plane wave. This means that instead of detecting young waves coming from close sources, the plane wave telescope is detecting the evolved mirror structures convected from upstream regions of the magnetosheath. These structures might have indeed reach a nonlinear regime and be distorted. In conclusion, the discrepancy is only apparent, the two tools are detecting different sets of waves present in the data.

Acknowledgements. The authors wish to thank C. Lacombe for interesting conversations and useful suggestions. This work was financially supported by the German Bundesministerium für Wirtschaft und Technologie and the Deutsches Zentrum für Luft und Raumfahrt under contract 50OC0103.

Topical Editor I. A. Daglis thanks M. Engebretson and another anonymous referee for their help in evaluating this paper.

References

Balikhin, M. A., de Wit, T. D., Alleyne, H. S. C. K., Wooliscroft, L. J. C., Walker, S. N., Krasnoselśkikh, V., Mier-Jedrzejeowicz, W. A. C., and Baumjohann, W.: Experimental determination of the dispersion of waves observed upstream of a quasi-perpendicular shock, Geophys. Res. Lett., 24, 787–790, doi:10.1029/97GL00671, 1997.

Balogh, A., Dunlop, M. W., Cowley, S. W. H., Southwood, D. J., Thomlinson, J. G., Glassmeier, K. H., Musmann, G., Luhr, H., Buchert, S., Acuña, M. H., Fairfield, D. H., Slavin, J. A., Riedler, W., Schwingenschuh, K., and Kivelson, M. G.: The Cluster Magnetic Field Investigation, Space Sci. Rev., 79, 65–91, 1997.

Blanco-Cano, X. and Schwartz, S. J.: Identification of low-frequency kinetic wave modes in the Earth's ion foreshock, Ann. Geophys., 15, 273–288, 1997, http://www.ann-geophys.net/15/273/1997/.

Capon, J., Greenfield, R. J., and Kloker, R. J.: Multidimensional maximum-likehood processing of a large aperture seismic array, in: Proc. IEEE, 55, 192–213, 1967.

Constantinescu, O. D., Glassmeier, K.-H., Motschmann, U., Treumann, R. A., and Fränz, M.: Plasma Wave Source Location Using CLUSTER as a Spherical Wave Telescope, available online at http://www.agu.org/journals/ja/, J. Geophys. Res., 111, doi:10.1029/2005JA011550, 2006.

Décréau, P. M. E., Fergeau, P., Krannosels'kikh, V., Leveque, M., Martin, P., Randriamboarison, O., Sene, F. X., Trotignon, J. G., Canu, P., and Mogensen, P. B.: Whisper, a Resonance Sounder and Wave Analyser: Performances and Perspectives for the Cluster Mission, Space Sci. Rev., 79, 157–193, 1997.

Escoubet, C. P., Schmidt, R., and Goldstein, M. L.: Cluster: Science and Mission Overview, Space Sci. Rev., 79, 11–32, 1997.

Glassmeier, K.-H., Motschmann, U., Dunlop, M., Balogh, A., Acuña, M. H., Carr, C., Musmann, G., Fornaçon, K.-H., Schweda, K., Vogt, J., Georgescu, E., and Buchert, S.: Cluster as a wave telescope – first results from the fluxgate magnetometer, Ann. Geophys., 19, 1439–1447, correction, Ann. Geophys., 21, 1071, 2003, 2001, http://www.ann-geophys.net/21/1071/2001/.

Hubert, D., Lacombe, C., Harvey, C. C., Moncuquet, M., Russell, C. T., and Thomsen, M. F.: Nature, properties, and origin of low-frequency waves from an oblique shock to the inner magnetosheath, J. Geophys. Res., 103, 26 783–26 798, doi:10.1029/98JA01011, 1998.

Johnstone, A. D., Alsop, C., Burge, S., Carter, P. J., Coates, A. J., Coker, A. J., Fazakerley, A. N., Grande, M., Gowen, R. A., Gurgiolo, C., Hancock, B. K., Narheim, B., Preece, A., Sheather, P. H., Winningham, J. D., and Woodliffe, R. D.: Peace: a Plasma Electron and Current Experiment, Space Sci. Rev., 79, 351–398, 1997.

Kasaba, Y., Matsumoto, H., Omura, Y., Anderson, R. R., Mukai, T., Saito, Y., Yamamoto, T., and Kokubun, S.: Statistical studies of plasma waves and backstreaming electrons in the terrestrial electron foreshock observed by Geotail, J. Geophys. Res., 105, 79–104, doi:10.1029/1999JA900408, 2000.

Lefeuvre, F. and Pinçon, J. L.: Determination of the wave-vector spectrum for plasma waves and turbulence observed in space plasmas, J. Atmos. Terr. Phys., 54, 1227–1235, 1992.

Motschmann, U., Woodward, T. I., Glassmeier, K.-H., and Dunlop, M. W.: Array Signal Processing Techniques, in: Proc. CLUSTER Workshop on Data Analysis Tools, edited by: Glassmeier, K.-H., Motschmann, U., and Schmidt, R., pp. 79–86, ESA, 1995.

Narita, Y. and Glassmeier, K.-H.: Dispersion analysis of low-frequency waves through the terrestrial bow shock, J. Geophys. Res. (Space Physics), 110, 12 215, doi:10.1029/2005JA011256, 2005.

Pillai, S. U.: Array signal processing, Springer, pp. 17–18, 1989.

Pinçon, J. L. and Lefeuvre, F.: Local characterization of homogeneous turbulence in a space plasma from simultaneous measurements of field components at several points in space, J. Geophys. Res., 96, 1789–1802, 1991.

Rème, H., Aoustin, C., Bosqued, J. M., Dandouras, I., Lavraud, B., Sauvaud, J. A., Barthe, A., Bouyssou, J., Camus, T., Coeur-Joly, O., Cros, A., Cuvilo, J., Ducay, F., Garbarowitz, Y., Medale, J. L., Penou, E., Perrier, H., Romefort, D., Rouzaud, J., Vallat, C., Alcaydé, D., Jacquey, C., Mazelle, C., D'Uston, C., Möbius, E., Kistler, L. M., Crocker, K., Granoff, M., Mouikis, C., Popecki, M., Vosbury, M., Klecker, B., Hovestadt, D., Kucharek, H., Kuenneth, E., Paschmann, G., Scholer, M., Sckopke, N., Sei-

denschwang, E., Carlson, C. W., Curtis, D. W., Ingraham, C., Lin, R. P., McFadden, J. P., Parks, G. K., Phan, T., Formisano, V., Amata, E., Bavassano-Cattaneo, M. B., Baldetti, P., Bruno, R., Chionchio, G., di Lellis, A., Marcucci, M. F., Pallocchia, G., Korth, A., Daly, P. W., Graeve, B., Rosenbauer, H., Vasyliunas, V., McCarthy, M., Wilber, M., Eliasson, L., Lundin, R., Olsen, S., Shelley, E. G., Fuselier, S., Ghielmetti, A. G., Lennartsson, W., Escoubet, C. P., Balsiger, H., Friedel, R., Cao, J.-B., Kovrazhkin, R. A., Papamastorakis, I., Pellat, R., Scudder, J., and Sonnerup, B.: First multispacecraft ion measurements in and near the Earth's magnetosphere with the identical Cluster ion spectrometry (CIS) experiment, Ann. Geophys., 19, 1303–1354, 2001,
http://www.ann-geophys.net/19/1303/2001/.

Sahraoui, F., Pinçon, J. L., Belmont, G., Rezeau, L., Cornilleau-Wehrlin, N., Robert, P., Mellul, L., Bosqued, J. M., Balogh, A., Canu, P., and Chanteur, G.: ULF wave identification in the magnetosheath: The k-filtering technique applied to Cluster II data, J. Geophys. Res., 108(A9), 1335, doi:10.1029/2002JA009587, 2003.

Sahraoui, F., Belmont, G., Pinçon, J., Rezeau, L., Balogh, A., Robert, P., and Cornilleau-Wehrlin, N.: Magnetic turbulent spectra in the magnetosheath: new insights, Ann. Geophys., 22, 2283–2288, 2004,
http://www.ann-geophys.net/22/2283/2004/.

Schwartz, S. J., Burgess, D., and Moses, J. J.: Low-frequency waves in the Earth's magnetosheath: present status, Ann. Geophys., 14, 1134–1150, 1996,
http://www.ann-geophys.net/14/1134/1996/.

Song, P., Russell, C. T., Gosling, J. T., Thomsen, M., and Elphic, R. C.: Observations of the density profile in the magnetosheath near the stagnation streamline, Geophys. Res. Lett., 17, 2035–2038, 1990.

Song, P., Russell, C. T., and Thomsen, M. F.: Slow mode transition in the frontside magnetosheath, J. Geophys. Res., 97, 8295–8305, 1992a.

Song, P., Russell, C. T., and Thomsen, M. F.: Waves in the inner magnetosheath – A case study, Geophys. Res. Lett., 19, 2191–2194, 1992b.

Tjulin, A., Pinçon, J.-L., Sahraoui, F., André, M., and Cornilleau-Wehrlin, N.: The k-filtering technique applied to wave electric and magnetic field measurements from the Cluster satellites, J. Geophys. Res. (Space Physics), 110, 11 224, doi:10.1029/2005JA011125, 2005.

Tsurutani, B. T. and Rodriguez, P.: Upstream waves and particles: An overview of ISEE results, J. Geophys. Res., 86, 4319–4324, doi:10.1029/0JGREA0000860000A6004319000001, 1981.

Walker, S., Sahraoui, F., Balikhin, M., Belmont, G., Pinçon, J., Rezeau, L., Alleyne, H., Cornilleau-Wehrlin, N., and André, M.: A comparison of wave mode identification techniques, Ann. Geophys., 22, 3021–3032, 2004,
http://www.ann-geophys.net/22/3021/2004/.